Modern Physics Letters B, Vol. 23, No. 9 (2009) 1129–1145

World Scientific
www.worldscientific.com

NOVEL PROPERTIES IN OXIDE HETEROSTRUCTURES

CHEN GE, KUI-JUAN JIN*, HUI-BIN LU and CONG WANG

Beijing National Laboratory for Condensed Matter Physics,
Institute of Physics, Chinese Academy of Sciences, Beijing 100190, China
**kjjin@aphy.iphy.ac.cn*

Received 18 March 2009

A brief review of recent investigations in oxide heterostructures is presented. First, experimental results are shown. Positive colossal magnetoresistance with high sensitivities are obtained at low magnetic field (<1000 Oe) nearly at room temperature. Picoseconds photoelectric effects of the rise time ∼210 ps and the half-maximum ∼650 ps are also found in some oxide heterostructures. Furthermore, resistance switching characteristic and electric displacement-voltage hysteresis loops have been observed in $BaTiO_{3-\delta}$/Si *p–n* heterostructures. Second, theoretical descriptions are also shown here. A model for the mechanism causing the positive colossal magnetoresistance has been established. Moreover, the transport properties and the important role played by oxygen vacancies are theoretically investigated in oxide heterostructures. In addition, an extended percolation model is well developed, with which the transport characteristic in oxide thin films can be well simulated based on the phase separation scenario. Notably, the interface effects play a crucial role in the multifunctional properties of the oxide heterostructures.

Keywords: Oxide heterostructures; positive magnetoresistance; picoseconds photoelectric effect.

1. Introduction

There has been a lot of interest in perovskite oxide heterostructures recently. Many novel phenomena have been reported in the past few years.[1–14] For example, it is rather amazing that two insulating oxides can form a superconducting interface layer.[1–3] Particularly, Tanaka *et al.* reported the electrical modulation of double-exchange ferromagnetism in the $La_{0.9}Ba_{0.1}MnO_3$/Nb-doped $SrTiO_3$ *p–n* junction.[5] Unusual positive CMR in *p–n* junction of $La_{0.9}Sr_{0.1}MnO_3$ (LSMO1) and $SrNb_{0.01}Ti_{0.99}O_3$ (SNTO) was also studied.[7] Not long ago, Vachhani *et al.* also showed some interesting results of positive colossal magnetoresistance (CMR) in the $La_{0.6}Pr_{0.2}Sr_{0.2}MnO_3$/Nb-$SrTiO_3$ junction.[8] Moreover, a lot of attention was paid to ultrafast picoseconds photoelectric characteristics of oxide heterostructures.[9] The ferroelectric response of $BaTiO_{3-\delta}$ (BTO) can be enhanced by the interface polarization of the junction.[10] At the same time, theoretical investigation in these systems

*Corresponding author.

have also been performed. The mechanism of the positive CMR is well presented.[11] Some researchers have shown a method of solving problems about transport in oxide heterostructures, and have proven that the trap energy levels induced by oxygen vacancies at the interface play an important role in transport.[13,14] In addition, an extended percolation model known as cluster percolation mode has been applied to explain the transport properties in oxide thin films based on the phase separation scenario.[12] In all, all of the issues mentioned above have been studied in structures with the interface. Effects of the interface should play a very important role in the multifunctional properties in the heterostructures and multilayers of perovskite oxide.

In this paper, a brief review of recent results on the perovskite oxide heterostructures is presented. Some experimental results are introduced in Sec. 2. Then, theoretical investigations about interesting experimental phenomena are shown in Sec. 3. Finally, we summarize our results in Sec. 4.

2. Experimental Results

2.1. *Unusual positive CMR in oxide heterostructures*

With the CMR effect discovered in junctions, scientists have taken great effort in fabricating appropriate structures and studying the physical origins for the characteristics. Magnetoresistance (MR) ratio is defined as $\Delta R/R_0 = (R_H - R_0)/R_0$, where R_H denotes the resistance under an applied magnetic field and R_0 denotes the resistance under a zero field. Some good CMR ratios are reported in magnetic tunnel junctions (MTJ), such as -150% in $La_{0.8}Sr_{0.2}MnO_3/SrTiO_3/La_{0.8}Sr_{0.2}MnO_3$ at 5 K under a low magnetic field (<10 Oe),[15] -450% in trilayer MTJ at 14 K in 200 Oe,[16] $+25\%$ at 80 K in 4 T in a $Fe_3O_4/SrTiO_3/La_{0.7}Sr_{0.3}MnO_3$ MTJ,[17] and a positive CMR at 48 K in 2 T in a $La_{0.7}Ca_{0.3}MnO_3/SrTiO_3/La_{0.7}Ce_{0.3}MnO_3$ MTJ.[4] It is noteworthy that only a few structures exhibit positive CMR properties. And most of them show characteristics at a low temperature or under a large magnetic field. Undoubtedly, they are hardly applied in microelectronic devices. Lately, not only a positive CMR but also a high CMR sensitivity with magnetic field at a high temperature is observed in a series of $La_{1-x}Sr_xMnO_3/SrNbyTi_{1-y}O_3$ heterostructures.[7] The ratios are observed to be as large as 11% in 5 Oe, 23% in 100 Oe, and 26% in 1000 Oe at 290 K; 53% in 5 Oe, 80% in 100 Oe, and 94% in 1000 Oe at 255 K. The CMR sensitivities are 85 Ω/Oe at 290 K, 246 Ω/Oe at 255 K, and 136 Ω/Oe at 190 K, respectively, with the applied magnetic field changed from 0 to 5 Oe.

A computer-controlled laser molecular-beam epitaxy (laser MBE) system was used to fabricate junctions.[18] The details of experiment can be found in Ref. 7. Transport measurements were carried out by a pulse-modulated current source, with pulse duration 1 s and the pulse interval 10 s. And the measuring current was smaller than 2 mA. All of these are to avoid the influence of the heating effect. The magnetic field was applied perpendicularly to the interface and superconductive

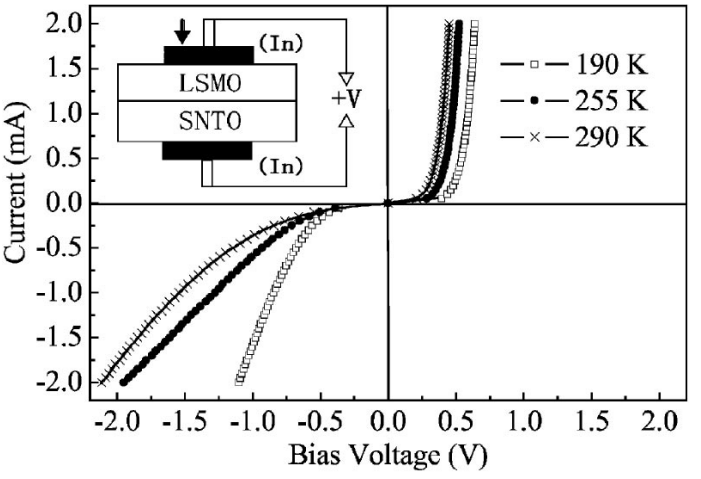

Fig. 1. The I–V curves of a LSMO1/SNTO junction at different temperatures. The schematic circuit of the sample measurement is shown in the inset.

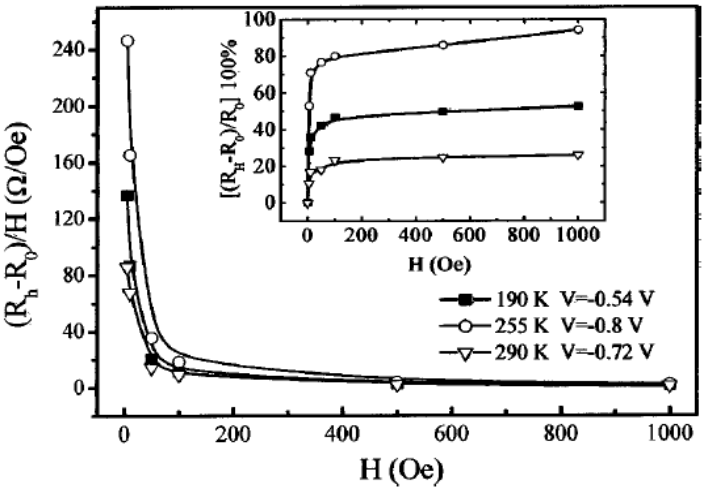

Fig. 2. The sensitivity of MR/H as a function of the magnetic field at optimal bias voltage. Inset: the MR ratios of the p–n junction as a function of the magnetic field at 290 K and $V_{\text{bias}} = -0.73$ V; 255 K and $V_{\text{bias}} = -0.80$ V; and 190 K and $V_{\text{bias}} = -0.54$ V.

quantum interference devices (SQUID, Quantum Design MPMS 5.5 T) were used to obtain magnetic properties. The I–V curves of LSMO1/SNTO at 190, 255, and 290 K are shown in Fig. 1.[7]

CMR variation and CMR ratios versus an applied magnetic fields are shown in Fig. 2 and its inset,[7] respectively. It can be concluded that the CMR sensitivities are rather high around room temperatures and under low magnetic fields. For example,

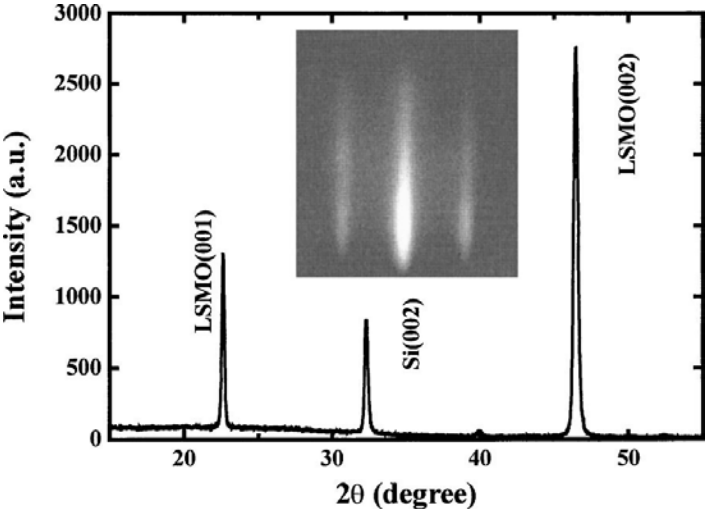

Fig. 3. A typical XRD pattern of 400 nm $LSMO_3$ film on Si substrate. The inset is a RHEED pattern of 400 nm $LSMO_3$ film on Si substrate.

the CMR sensitivities are 85 Ω/Oe at 290 K, 246 Ω/Oe at 255 K, and 136 Ω/Oe at 190 K, with a small change from 0 to 5 Oe. More details can be seen in Fig. 2. Obviously, this is of great value in terms of designing new devices.

We know that doped $LaMnO_3$ compounds exhibit negative MR, while $SrTiO_3$ hardly shows any MR property. Therefore, it is indeed amazing that the junction fabricated by LSMO1 and SNTO has a positive CMR. The physical origin of the positive CMR has been clearly explained by a model, which will be presented in Sec. 3.1.

2.2. *Ultrafast picoseconds photoelectric effect*

Many efforts have been taken to investigate laser induced properties of heterojunctions for many years.[19,20] A picoseconds photoelectric phenomenon in $La_{0.7}Sr_{0.3}MnO_3$ (LSMO3)/Si junction was reported,[9] which gave an impetus to ultrafast photovoltaic researches.

This structure is also fabricated using Laser MBE. Details about junction preparation can be found in Ref. 9. An X-ray diffraction (XRD) analysis is performed in Fig. 3,[9] which shows that LSMO3 film is *c*-axis oriented and grown with a two-dimensional layer-by-layer growth mode. Furthermore, the I–V curve exhibits excellent nonlinear and rectifying characteristics in this system.

The photoelectric behaviors of LSMO3/Si p–n junctions were investigated using a 1064 nm Nd:YAG laser (pulse width 25 ps) as well as a 10.6 mm CO_2 pulse laser and measured by an oscilloscope of 130 ps rise time (Tektronix® TDS7254B) at ambient temperature. Figure 4[9] shows a photoelectric response of an open-circuit system. The rise time is about 10 ns and the FWHM is about 12 μs. More excitingly,

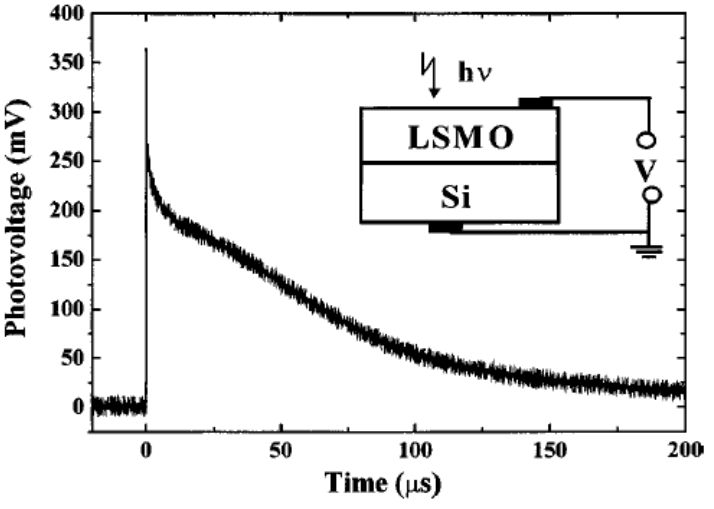

Fig. 4. Variation of the open-circuit photovoltage with time after excitation with a 1064 nm laser pulse on the LSMO3/Si p–n junction. The schematic circuit of the sample measurement is shown in the inset.

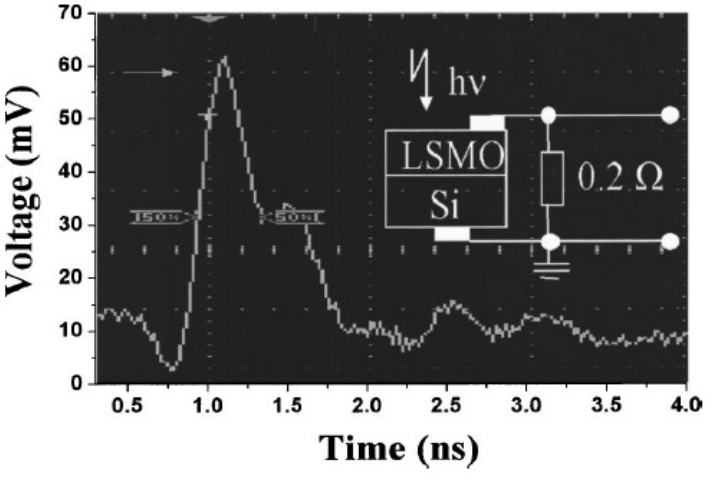

Fig. 5. Variation of the photovoltage with time under the same condition as in Fig. 4 but with a 0.2 Ω resistance connected in parallel across the p–n junction. Inset displays a schematic circuit of the sample measurement.

a picoseconds photoelectric behavior is observed in a system parallel with a 0.2 Ω resistance, shown in Fig. 5.[9] The rise time dramatically reduces to 210 ps and the FWHM also reduces to 650 ps.

There are two main factors influencing the rise time and FWHM of the photovoltaic effect in Fig. 4. One is the quality of the interface between two different

materials. Many defects can affect the response severely. The other is the junction capacitance in the LSMO3/Si and the impedance of the measurement system. In the present case, the junction capacitance is about 30 pF at 500 MHz for the LSMO3/Si sample of 5×6 mm^2, and the input impedance of the oscilloscope is 1 MΩ. In other words, the discharge time constant is about 30 ms, which is comparable to the FWHM of the photovoltaic pulse in Fig. 4. Hence, Fig. 5 reveals a more realistic process of photoelectric effects in this system.

The fact that the junction irradiated by a 10.6 μm CO_2 laser pulse, for which the photon energy is much smaller than either of the band gap of the LSMO3 or Si, did not show any photovoltage signal, excludes a thermoelectric effect in evidence. Finally, this feature can be well used in high speed photoelectric devices.

2.3. *Resistance switching in BTO/Si p–n heterostructure*

Recently, the resistive hysteresis effect, which reflects resistance switching under external stimuli, has attracted wide attention due to its potential applications in nonvolatile resistance memory.[21] In previous work, the ferroelectric hysteresis loop was observed in $BaNb_{0.3}Ti_{0.7}O_3$/Si p–n junction.[22] Lately, not only the electric displacement–voltage (D–V) hysteresis loop but also more interesting hysteresis I–V characteristics have been found in the BTO/Si p–n junction.

BTO thin films were epitaxially grown on p-type Si substrates under a low oxygen pressure. The resistance switching characteristic was observed in BTO/Si p–n junctions. As shown in Fig. 6,[10] the voltage was swept as $-6 \rightarrow 0 \rightarrow +6 \rightarrow 0 \rightarrow -6$ V and the numbers from 1 to 4 indicate the direction of the voltage sweep. It

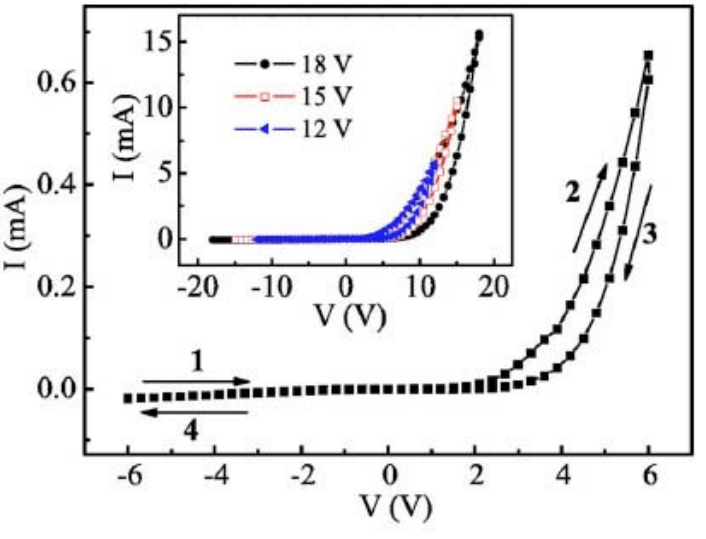

Fig. 6. Hysteresis I–V characteristic of BTO/Si p–n junction. The inset shows the hysteresis I–V curves of the junction under various V_{max}.

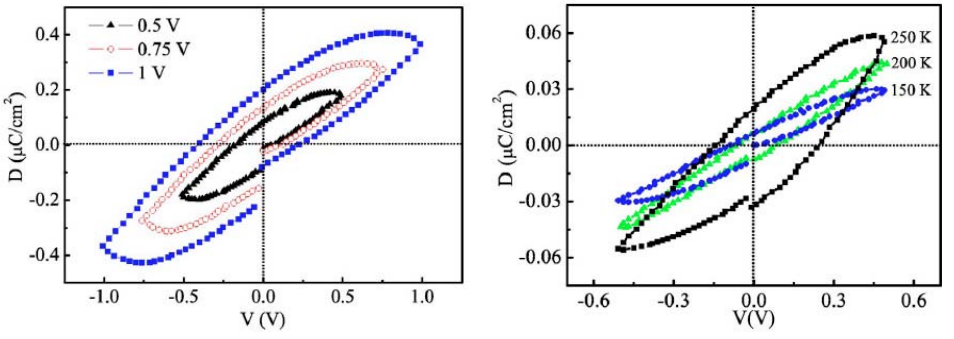

(a) (b)

Fig. 7. (a) The D–V loops of BTO/Si p–n junction at three different applied voltages. (b) The D–V loops of BTO/Si p–n junction at different temperatures.

can be clearly seen that the junction exhibits a low resistance state when sweeping voltage from 0 to + 6 V, and exhibits a high resistance state when sweeping voltage from + 6 to 0 V. Hysteresis I–V characteristics for different $V_{\max}$ are also measured. As shown in the inset of Fig. 6, all the I–V curves exhibit similar hysteresis properties.

The polarization related resistance modulation is usually observed in some ferroelectric films and heterostructures.[23,24] The D–V loops of the BTO/Si p–n junction with different applied voltages are measured, as shown in Fig. 7(a).[10] It can be seen that the area of the hysteresis loops become greater under larger applied voltages. This verifies that the resistance switching is related to ferroelectric response. To prove whether the D–V hysteresis loops resulted from BTO thin film, BTO thin film on $SrRuO_3/SrTiO_3$ (SRO/STO) substrate under the same deposition conditions as those for the $BaTiO_3$/Si p–n junction is also grown. The hysteresis loop in the BTO thin film on SRO/STO substrate is not observed, in which the SRO is metallic.[25] The temperature-dependent hysteresis loops of the BTO/Si heterostructure are shown in Fig. 7(b).[10] The BTO/Si junction exhibits weaker ferroelectric response in lower temperature. It cannot be understood only by the ferroelectric property of BTO. Because the resistivity of BTO is increased with decreasing temperature, the BTO thin film is supposed to exhibit stronger ferroelectric response in lower temperature due to the decrease of leakage current. Thus, the interface may play an important role in this system.

In BTO/Si structure, there is a potential barrier at the interface due to the diffusion of carriers. And equal positive charges and negative charges appear in the n region and p region, respectively. The dipole moments at the interface can give rise to polarization enhancement in BTO/Si p–n junction.[26,27] With increasing positive bias voltage, the positive polarization of BTO increases. Then, as the bias voltage decreases from $V_{\max}$, the polarization of BTO also decreases. As shown in Fig. 7(a), the magnitude of polarization in the polarization process 0 to $V_{\max}$ is smaller than

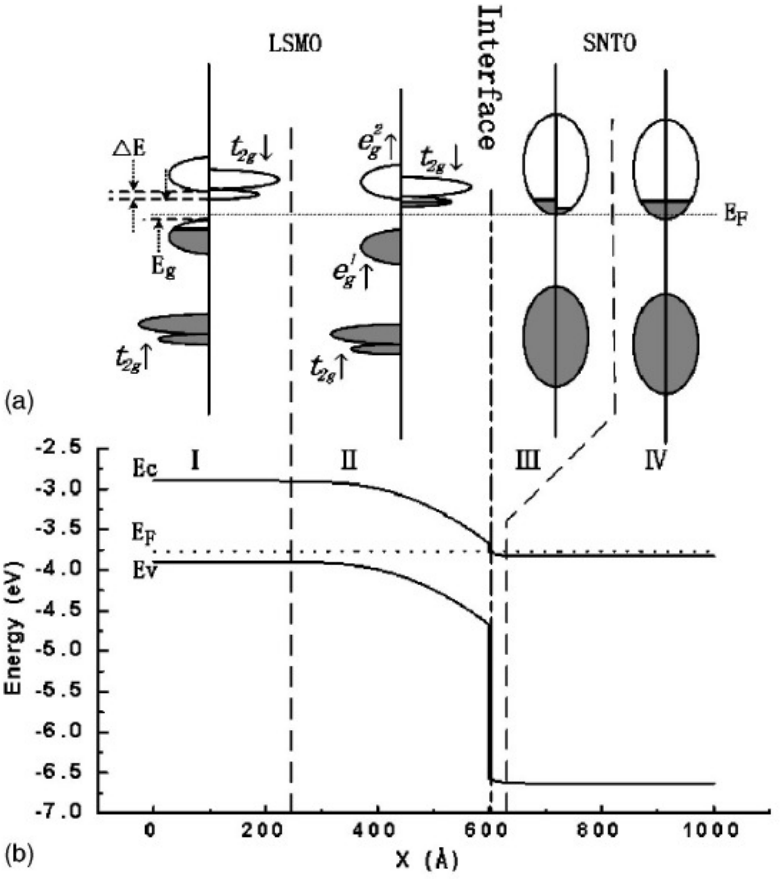

Fig. 8. (a) The schematic DOS of the junction, and (b) the band diagram for each region obtained by self-consistent calculation.

its counterpart in the depolarization process $V_{\max}$ to 0 due to the hysteresis effect of polarization versus applied voltage. Therefore, this interesting resistance switching property may be well explained in terms of the interface polarization.

In all, these interesting results suggest the possibility of a wide study on resistance switching devices based on oxide and Si p–n junctions.

3. Theoretical Descriptions

3.1. *The mechanism of positive CMRs*

A model was proposed to explain the physical origin of unusual positive CMR. Self-consistent calculation has been carried out. The calculated band structure and the schematic density of state of LSMO1/SNTO are plotted in Fig. 8.[11]

At the reverse bias voltage and under an applied magnetic field, electrons in the $e_g^1\uparrow$ band of region I can fill up the $t_{2g}\downarrow$ band of region II, which induces a large resistance (causing the positive MR). Similarly, because of a small band gap between the bottom of $t_{2g}\downarrow$ and $e_g^2\uparrow$ bands and an applied negative voltage, electrons in the $e_g^1\uparrow$ band of region I can even move into the $e_g^2\uparrow$ band of region II, which induces a small resistance (causing the negative MR). The total MR manifests the result of competitions between interband tunneling from the $e_g^1\uparrow$ band to the $t_{2g}\downarrow$ band, and from the $e_g^1\uparrow$ band to the $e_g^2\uparrow$ band.

Based on the above discussions, ΔI_+ (causing the positive MR) and ΔI_- (causing the negative MR) can be simply expressed as Eqs. (1) and (2), where $\mathrm{DOS_I}(E_{e^1\uparrow})$, $\mathrm{DOS_{II}}(E_{t\downarrow})$ and $\mathrm{DOS_{II}}(E_{e^2\uparrow})$ denote the density of states (DOS) in the $e_g^1\uparrow$ band of region I, the $t_{2g}\downarrow$ band of region II and the $e_g^2\uparrow$ band of region II, respectively:

$$\Delta I_+ = I_+^0 - I_+^H \propto \mathrm{DOS_I}(E_{e^1\uparrow})^*\mathrm{DOS_{II}}(E_{t\downarrow})\,, \tag{1}$$

$$\Delta I_- = I_-^H - I_-^0 \propto \mathrm{DOS_I}(E_{e^1\uparrow})^*\mathrm{DOS_{II}}(E_{e^2\uparrow})\,. \tag{2}$$

Figure 9[11] shows the variation of CMR values of the system with the negative bias voltage under various magnetic fields at three different temperatures. This model can successfully explain the physics in Fig. 9 from three different aspects. Firstly, under the same temperature and magnetic field, at a low reverse bias voltage, electrons in the $e_g^1\uparrow$ band of region I mainly tunnel into the $t_{2g}\downarrow$ band of region II, which leads to a positive MR. With the reverse bias voltage increased, the Fermi level in region II is lifted higher, making ΔI_+ larger. Eventually, when the reverse bias voltage reaches a point at which electrons tunneling from the $e_g^1\uparrow$ band of region I to the $e_g^2\uparrow$ band of region II cannot be neglected, the MR reaches peak value. Then, the total MR will decrease, if the bias continues to increase. However, the whole MR will not show negative MR, until ΔI_- is bigger than ΔI_+. Secondly, at the same temperature and reverse bias voltage, the MR will change with the magnetic field altered as follows. The spin polarization of the majority carriers in region I and the spin polarization of the minority carriers in region II, with the increase of the magnetic field, are both increased. Thus, less current can be carried from region I to region II due to the scattering between carriers of antiparallel spins. In other words, the resistance is larger in this structure. Thirdly, the temperature dependence of positive MR can also be understood well. With the increased temperature, the electron filling of the $t_{2g}\downarrow$ band of region II increases, as well as the positive MR in the system (190–255 K). However, after the filling of electrons in region II reaches the edge of the $e_g^2\uparrow$ band, the positive MR decreases (255–290 K).

Furthermore, some numerical simulations have been carried out according to this model.[14,28–31] Thus, the model, which grasps the main physics in this system, has been further developed.

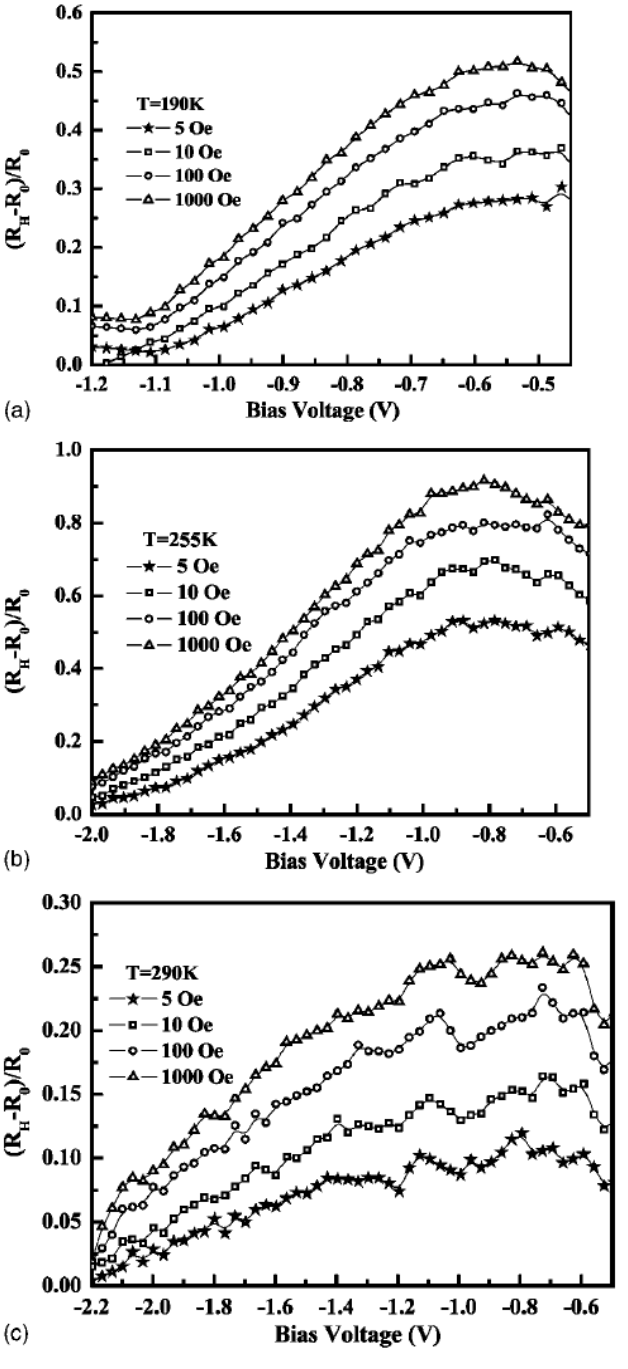

Fig. 9. The variation of MR values of the system with the negative bias voltage under several values of the applied magnetic field at the temperatures of (a) 190 K, (b) 255 K and (c) 290 K.

3.2. *The cluster percolation mode*

Experimentally, the phase separation phenomenon, observed in many systems of manganites,[32–35] has been considered as an intrinsic inhomogeneity. Moreover, it is found that the resistivity of thin film has a more abrupt character change near the metal-to-insulator transition (MIT),[36] compared with that of bulk material.[32,37–39] Some qualitative theoretical simulations have been performed to explain this strange and interesting phenomenon.[40,41] A model was developed,[12] called the cluster percolation mode, to interpret the physical mechanism of this extraordinary abrupt change based on percolation model.[42]

The system, regarded as a two-dimensional (2D) $N \times N$ matrix, is composed of an FM metallic phase with resistance $R_M(T)$ and a PM insulating phase with resistance $R_I(T)$. A quantity f, defined as $f =$ (the number of FM lattice sites)/(the total number of lattice sites), is in the form of a Fermi distribution-like function. To calculate $R_M(T)$ and $R_I(T)$, $\rho_m(T) = \rho_{m0} + \rho_{m1}T^2 + \rho_{m2}T^{4.5}$ and $\rho_i(T) = \rho_{i0}\exp[E_0/(k_BT)]$ are assumed, where ρ_{m0} is the residual resistivity at $T \sim 0$ K, the T^2 term indicates the electron scattering with the coefficient ρ_{m1},[43] the $T^{4.5}$ term denotes the magnon scattering involving the phonon scattering with the coefficient ρ_{m2},[44] the coefficient ρ_{i0} is the high-T residual resistivity and E_0 is the activation energy. Using the Breadth First Traversal algorithm,[45] the path lengths of the metallic and insulating domains are found to calculate $R_M(T)$ and $R_I(T)$. Hence, the effective resistivity is gained.

In the standard percolation mode, the occupation of the square is random. It is applied into the simulation of T-dependent resistivity of $La_{0.9}Te_{0.1}MnO_3$ bulk, shown in Fig. 10.[12] Choices of various parameters can be found in Ref. 12. The excellent accordance between simulations and experiments proves that the standard percolation mode is fairly suitable for the simulation of bulk resistivity.

Simultaneously, the standard percolation mode is used in the simulation of ρ–T curves of $La_{0.9}Te_{0.1}MnO_3$ thin films, shown as a dashed line in Fig. 11.[12] Details about parameters can be found in Ref. 12. Obviously, the main abrupt change property in thin films is not simulated well. Therefore, some modifications must be done in the standard percolation mode for thin films. It is assumed that the square is correlated with the status of its neighbors. When T is increased, only those FM sites which have at least one PM neighbor can turn into PM squares, resulting in the growth of the PM domain. This kind of percolation mode is called the cluster percolation mode. So, it is easily concluded that the main difference between these two modes lies in the variation of domain size and domain number under the temperature evolution. With the temperature increased, the cluster percolation mode reveals a process in which the PM domain size increases but the domain number stays unchanged, while the standard percolation demonstrates a process in which the domain size is nearly unchanged but the domain number increases. The results in the cluster percolation mode are presented as a solid line in Fig. 11. It is wonderfully identical to the experiment result. A similar simulation about

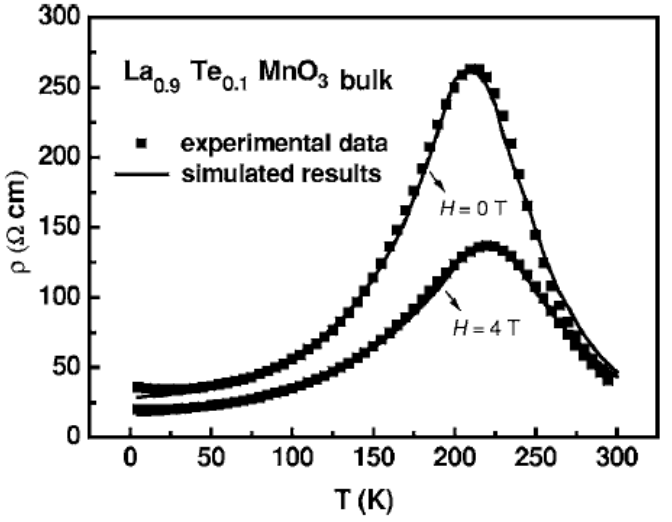

Fig. 10. Simulated T-dependent resistivity (solid lines) of $La_{0.9}Te_{0.1}MnO_3$ bulk compared with the experimental data (full circles) with and without H, respectively.

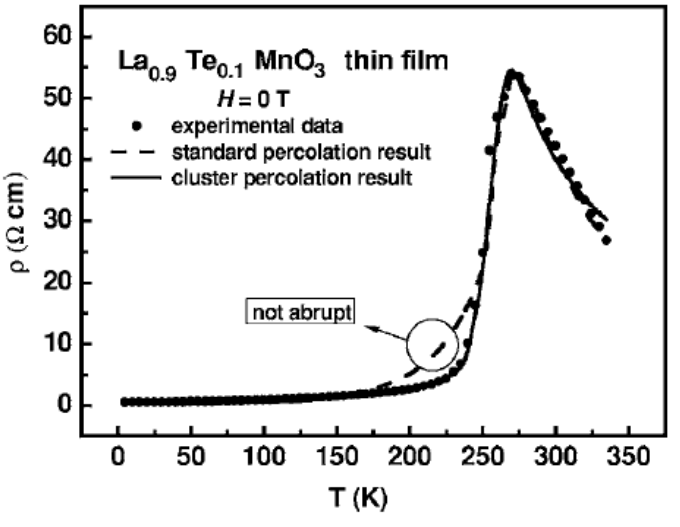

Fig. 11. Simulated result of the T-dependent resistivity obtained by cluster percolation (solid line) for $La_{0.9}Te_{0.1}MnO_3$ thin film without H.

$La_{2/3}Ca_{1/3}MnO_3$ thin films is also performed and the result shows that the cluster percolation mode indeed well explains the T-dependent resistance of thin films. More applications and researches about the cluster percolation can be found in Refs. 46–48.

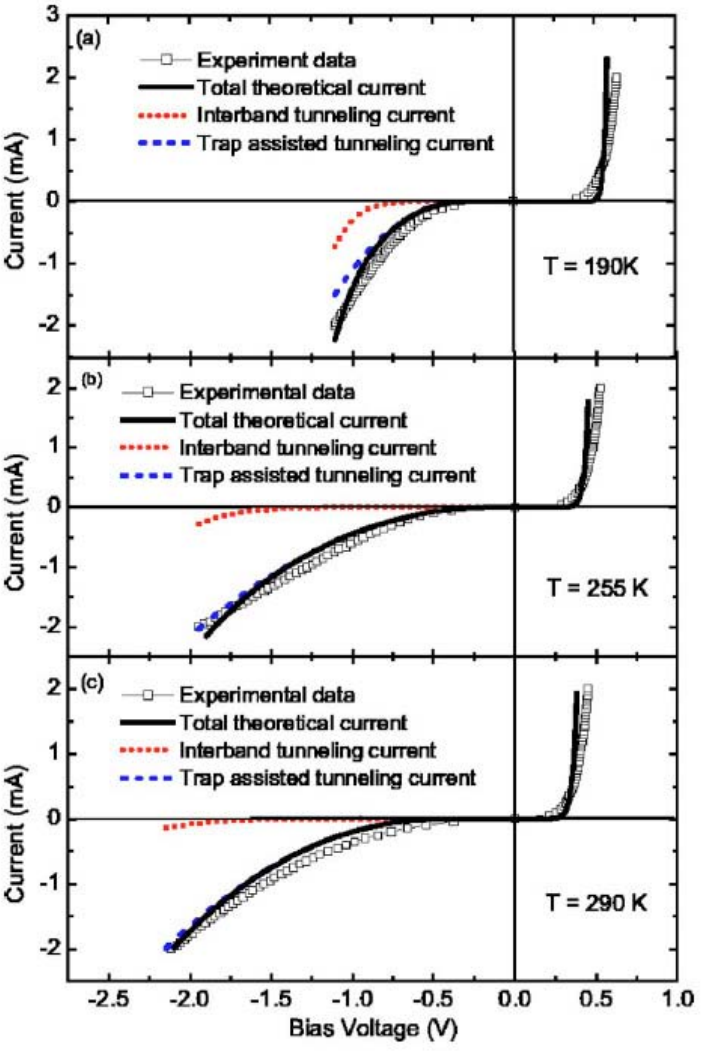

Fig. 12. The theoretical results versus experimental data from reverse bias to forward bias with (a) $T = 190$ K, (b) $T = 255$ K, and (c) $T = 290$ K, respectively. In these figures, the solid, dashed, and dotted curves represent the interband, Zener tunneling current, trap assisted tunneling current, and total theoretical current, respectively. The hollow squares describe the experimental data.

3.3. *The mechanism of transport properties in perovskite oxide heterojunctions*

Although the I–V curves in LSMO1/SNTO junction are shown in Fig. 1, the details of the transport properties are not clear yet. Thus, the study on mechanisms is very necessary. Some studies on the mechanism of transport properties in LSMO1/SNTO junction have been reported.[13]

Because the hole-doped LSMO1 is a multicorrelated ferromagnetic semiconductor,[5,49] and the coulomb repulsion among electrons in the multicorrelated system is much weaker than that in the strong-correlated system, this provides the possibility to analyze the transport characteristics of multicorrelated devices by using conventional semiconductor band theory. Thus, the transport properties of the LSMO1/SNTO were analyzed based on self-consistent calculations of Poisson equation and the drift-diffusion formulation as Eq. (3):

$$\begin{aligned} -\frac{d^2\phi(x)}{dx^2} &= \frac{q}{\varepsilon}[p(x) - n(x) - N_a + N_d]\,, \\ D_n\frac{d^2n(x)}{dx^2} - \mu_n\frac{d\phi(x)}{dx}\frac{dn(x)}{dx} - \mu_n n(x)\frac{d^2\phi(x)}{dx^2} &= R(x)\,, \\ D_p\frac{d^2p(x)}{dx^2} + \mu_p\frac{d\phi(x)}{dx}\frac{dp(x)}{dx} + \mu_p p(x)\frac{d^2\phi(x)}{dx^2} &= R(x)\,. \end{aligned} \tag{3}$$

The Richardson current is adopted at the interface in this system. When the reverse bias voltage is applied, interband Zener tunneling current is considered. In addition, it is proved that the trap assisted tunneling process, assisted by the oxygen vacancy induced states in the forbidden gap,[50] is rather important when the applied negative voltage is low. The trap assisted tunneling current J_{TAT} can be represented as Eq. (4), where $N(E)$ denotes the densities of states and $F(E)$ describes the Fermi distribution function. N_t presents the density of traps and σ_t is the effective capture cross section. The values of $Nt\sigma_t$ are taken as 0.15, 0.75 and 1.0 at $T = 190$, 255 and 290 K, respectively. The tunneling rates of this two-step process $T_1(E)$ and $T_2(E)$ are obtained with the method given in Refs. 51 and 52.

$$J_{\mathrm{TAT}} = qN_t\sigma_t\int_{E_{Fn}}^{E_{vp}} N(E)F(E)\frac{T_1(E)T_2(E)}{T_1(E)+T_2(E)}dE\,. \tag{4}$$

As shown in Fig. 12,[13] the figures of theoretical calculation are consistent with the experimental results. In particular, this work is of great value in two areas: an effective method has been presented to simulate the transport process in this oxide system; oxygen vacancies can strongly affect transport properties. And especially, the trap energy levels induced by oxygen vacancies at the interface must be considered carefully.

In all, the drift-diffusion process is the dominant transport mechanism in oxide heterostructures with forward bias, and the interband Zener tunneling current plays an important role in the reversed transport process with high reverse bias. In addition to conventional semiconductor theory, the trap assisted tunneling process, induced by oxygen vacancies, is the main mechanism for the leakage current in the oxide junction at low reverse bias.

4. Conclusion

We have presented a brief review of recent achievements on perovskite oxide heterostructures. First, some interesting experimental results are shown in Sec. 2, such as large positive MR with high sensitivities, picoseconds ultrafast photoelectric effect, and resistance switching property in oxide heterostructures. Some results should be of great value for designing new devices based on oxide. Second, some theoretical considerations are reviewed. Some models for positive MR, the T-dependent resistivity in oxide thin film, and transport properties of oxide heterojunctions, are shown. We have found that the filling up of the minority carriers around the interface is the main origin for positive MR. And that the trap levels induced by the oxygen vacancies adjacent to the interface can greatly affect the transport properties. An extended percolation model is also developed to simulate the abrupt change of the T-dependent resistivity. In particular, effects of the interface should play a very important role in the heterostructures and multilayers of perovskite oxide.

Acknowledgment

The authors acknowledge the financial support from the National Natural Science Foundation of China and the National Basic Research Program of China.

References

1. A. Ohtomo and H. Y. Hwang, *Nature* **427** (2004) 423.
2. W. Siemons, G. Koster, H. Yamamoto, W. A. Harrison, G. Lucovsky, T. H. Geballe, D. H. A. Blank and M. R. Beasley, *Phys. Rev. Lett.* **98** (2007) 196802.
3. K. Ueno, S. Nakamura, H. Shimotani, A. Ohtomo, N. Kimura, T. Nojima, H. Aoki, Y. Iwasa and M. Kawasaki, *Nature Mater.* **7** (2008) 855.
4. C. Mitra, P. Raychaudhuri, K. Dorr, K. H. Muller, L. Schultz, P. M. Oppeneer and S. Wirth, *Phys. Rev. Lett.* **90** (2003) 017202.
5. H. Tanaka, J. Zhang and T. Kawai, *Phys. Rev. Lett.* **88** (2002) 027204-1.
6. H. B. Lu, G. Z. Yang, Z. H. Chen, S. Y. Dai, Y. L. Zhou, K.-J. Jin, B. L. Cheng, M. He, L. F. Liu, Y. Y. Fei, W. F. Xiang and L. Yan, *Appl. Phys. Lett.* **84** (2004) 5007.
7. H. B. Lu, S. Y. Dai, Z. H. Chen, Y. L. Zhou, B. L. Cheng, K.-J. Jin, L. F. Liu and G. Z. Yang, *Appl. Phys. Lett.* **86** (2005) 032502.
8. P. S. Vachhani, J. H. Markna, D. G. Kuberkar, R. J. Choudhary and D. M. Phase, *Appl. Phys. Lett.* **92** (2008) 043506.
9. H. B. Lu, K.-J. Jin, Y. H. Huang, M. He, K. Zhao, B. L. Cheng, Z. H. Chen, Y. L. Zhou, S. Y. Dai and G. Z. Yang, *Appl. Phys. Lett.* **86** (2005) 241915.
10. G. Z. Liu, K.-J. Jin, J. Qiu, M. He, H. B. Lu, J. Xing, Y. L. Zhou and G. Z. Yang, *Appl. Phys. Lett.* **91** (2007) 252110.
11. K.-J. Jin, H. B. Lu, Q. L. Zhou, K. Zhao, B. L. Cheng, Z. H. Chen, Y. L. Zhou and G. Z. Yang, *Phys. Rev. B* **71** (2005) 184428.
12. Q. L. Zhou, K.-J. Jin, K. Zhao, D. Y. Guan, H. B. Lu, Z. H. Chen and G. Z. Yang, *Phys. Rev. B* **72** (2005) 224439.
13. P. Han, K.-J. Jin, H. B. Lu, Q. L. Zhou, Y. L. Zhou and G. Z. Yang, *Appl. Phys. Lett.* **91** (2007) 182102.

14. Q. L. Zhou, K.-J. Jin, H. B. Lu, P. Han, Z. H. Chen, K. Zhao, Y. L. Zhou and G. Z. Yang, *Europhys. Lett.* **71** (2005) 283.
15. T. Obata, T. Manako, Y. Shimakawa and Y. Kubo, *Appl. Phys. Lett.* **74** (1999) 290.
16. J. O'Donnell, A. E. Andrus, S. Oh, E. V. Colla and J. N. Eckstein, *Appl. Phys. Lett.* **76** (2000) 1914.
17. K. Ghosh, S. B. Ogale, S. P. Pai, M. Robson, E. Li, I. Jin, Z. W. Dong, R. L. Greene, R. Ramesh, T. Venkatesan and M. Johnson, *Appl. Phys. Lett.* **73** (1998) 689.
18. G. Z. Yang, H. B. Lu, Z. H. Chen, D. F. Cui, H. S. Wang, H. Q. Yang, F. Y. Miao, Y. L. Zhou and L. Li, *Sci. China, Ser. A: Math. Phys. Astron.* **28** (1998) 260.
19. P. X. Zhang, W. K. Lee and G. Y. Zhang, *Appl. Phys. Lett.* **81** (2002) 4026.
20. J. R. Sun, C. M. Xiong, B. G. Shen, P. Y. Wang and Y. X. Weng, *Appl. Phys. Lett.* **84** (2004) 2611.
21. M. P. Singh, L. Méchin, W. Prellier and M. Maglione, *Appl. Phys. Lett.* **89** (2006) 202906.
22. Y. H. Huang, K. Zhao, H. B. Lu, K.-J. Jin, M. He, Z. H. Chen, Y. L. Zhou and G. Z. Yang, *Appl. Phys. Lett.* **88** (2006) 061919.
23. P. W. M. Blom, R. M. Wolf, J. F. M. Cillessen and M. P. C. M. Krijn, *Phys. Rev. Lett.* **73** (1994) 2107.
24. D. J. Fu, J. C. Lee, S. W. Choi, S. J. Lee, T. W. Kang, M. S. Jang, H. I. Lee and Y. D. Woo, *Appl. Phys. Lett.* **81** (2002) 5207.
25. C. L. Chen, Y. Cao, Z. J. Huang, Q. D. Jiang, Z. Zhang, Y. Y. Sun, W. N. Kang, L. M. Dezaneti, W. K. Chu and C. W. Chu, *Appl. Phys. Lett.* **71** (1997) 1047.
26. I. B. Misirlioglu, M. Alexe, L. Pintilie and D. Hesse, *Appl. Phys. Lett.* **91** (2007) 022911.
27. C. G. Duan, R. F. Sabirianov, W. N. Mei, S. S. Jaswal and E. Y. Tsymbal, *Nano Lett.* **6** (2006) 483.
28. C. L. Hu, K.-J. Jin, H. B. Lu, L. Liao and G. Z. Yang, *Solid State Commun.* **149** (2009) 334.
29. C. L. Hu, P. Han, K.-J. Jin, H. B. Lu and G. Z. Yang, *J. Appl. Phys.* **103** (2008) 053701.
30. C. L. Hu, K.-J. Jin, P. Han, H. B. Lu, L. Liao and G. Z. Yang, *Appl. Phys. Lett.* **93** (2008) 162106.
31. J. Qiu, K.-J. Jin, P. Han, H. B. Lu, C. L. Hu, B. P. Wang and G. Z. Yang, *Europhys. Lett.* **79** (2007) 57004.
32. M. Uehara, S. Nori, C. H. Chen and S. W. Cheong, *Nature* **399** (1999) 560.
33. J. M. De Teresa, M. R. Ibarra, P. A. Algarabel, C. Ritter, C. Marquina, J. Blasco, J. García, A. del Moral and Z. Arnold, *Nature* **386** (1997) 256.
34. L. Zhang, C. Israel, A. Biswas, R. L. Greene and A. de Lozanne, *Science* **298** (2002) 805.
35. M. Fäth, S. Freisem, A. A. Menovsky, Y. Tomioka, J. Aarts and J. A. Mydosh, *Science* **285** (1999) 1540.
36. X. T. Zeng and H. K. Wong, *Appl. Phys. Lett.* **72** (1998) 740.
37. G. T. Tan, S. Dai, P. Duan, Y. L. Zhou, H. B. Lu and Z. H. Chen, *Phys. Rev. B* **68** (2003) 014426.
38. G. T. Tan, S. Y. Dai, P. Duan, Y. L. Zhou, H. B. Lu and Z. H. Chen, *J. Appl. Phys.* **93** (2003) 5480.
39. R. Mahendiran, S. K. Tiwary, A. K. Raychaudhuri, T. V. Ramakrishnan, R. Mahesh, N. Rangavittal and C. N. R. Rao, *Phys. Rev. B* **53** (1996) 3348.
40. M. Mayr, A. Moreo, J. A. Vergés, J. Arispe, A. Feiguin and E. Dagotto, *Phys. Rev. Lett.* **86** (2001) 135.

41. J. Burgy, E. Dagotto and M. Mayr, *Phys. Rev. B* **67** (2003) 014410.
42. D. Stauffer, *Introduction to Percolation Theory* (Taylor & Francis, London and Philadelphia, 1985).
43. A. H. Thompson, *Phys. Rev. Lett.* **35** (1975) 1786.
44. K. Kubo and N. Ohata, *J. Phys. Soc. Jpn.* **33** (972) 21.
45. S. Skiena, *Implementing Discrete Mathematics: Combinatorics and Graph Theory with Mathematica* (Addison-Wesley, California, 1990).
46. Q. L. Zhou, K. Zhao, K.-J. Jin, D. Y. Guan, H. B. Lu, Z. H. Chen, G. Z. Yang, A. Li and H. K. Wong, *Appl. Phys. Lett.* **87** (2005) 172510.
47. Q. L. Zhou, K.-J. Jin, D. Y. Guan, Z. H. Chen, H. B. Lu and G. Z. Yang, *Phys. Lett. A* **350** (2006) 283.
48. Q. L. Zhou, D. Y. Guan, K.-J. Jin, K. Zhao, Z. H. Chen, H. B. Lu, Y. L. Zhou, P. Han and G. Z. Yang, *Chin. Phys. Lett.* **22** (2005) 1749.
49. E. Dagotto, T. Hotta and A. Moreo, *Phys. Rep.* **344** (2001) 1.
50. S. Picozzi, C. Ma, Z. Yang, R. Bertacco, M. Cantoni, D. Petti, S. Brivio and F. Ciccacci, *Phys. Rev. B* **75** (2007) 094418.
51. O. Pinaud, *J. Appl. Phys.* **92** (2002) 1987.
52. A. El. Ayyadi and A. Jüngel, *SIAM J. Appl. Math.* **66** (2006) 554.